

Population of tetraneutron continuum in reactions of ^8He on deuterium

I.A. Muzalevskii,^{1,*} N.B. Shulgina,^{2,3} A.A. Bezbakh,^{1,4} V. Chudoba,^{1,4} S.A. Krupko,¹ S.G. Belogurov,^{1,5} D. Biare,¹ I.A. Egorova,¹ A.S. Fomichev,^{1,6} E.M. Gazeeva,¹ A.V. Gorshkov,¹ L.V. Grigorenko,^{1,5,2} G. Kaminski,^{1,7} M. Khirk,^{8,1} O. Kiselev,⁹ D.A. Kostyleva,^{9,10} M.Yu. Kozlov,¹¹ B. Mauryey,^{1,12} I. Mukha,⁹ E.Yu. Nikolskii,^{2,1} Yu.L. Parfenova,¹ W. Piatek,^{1,7} A.M. Quynh,^{1,13} V.N. Schetinin,¹¹ A. Serikov,¹ S.I. Sidorchuk,¹ P.G. Sharov,^{1,4} R.S. Slepnev,¹ S.V. Stepanyov,¹ A. Swiercz,^{1,14} P. Szymkiewicz,^{1,14} G.M. Ter-Akopian,^{1,6} and B. Zalewski^{1,7}

¹*Flerov Laboratory of Nuclear Reactions, JINR, 141980 Dubna, Russia*

²*National Research Centre “Kurchatov Institute”, Kurchatov sq. 1, 123182 Moscow, Russia*

³*Bogoliubov Laboratory of Theoretical Physics, JINR, 141980 Dubna, Russia*

⁴*Institute of Physics, Silesian University in Opava, 74601 Opava, Czech Republic*

⁵*National Research Nuclear University “MEPhI”, 115409 Moscow, Russia*

⁶*Dubna State University, 141982 Dubna, Russia*

⁷*Heavy Ion Laboratory, University of Warsaw, 02-093 Warsaw, Poland*

⁸*Skobeltsyn Institute of Nuclear Physics, Moscow State University, 119991 Moscow, Russia*

⁹*GSI Helmholtzzentrum für Schwerionenforschung GmbH, 64291 Darmstadt, Germany*

¹⁰*II. Physikalisches Institut, Justus-Liebig-Universität, 35392 Giessen, Germany*

¹¹*Laboratory of Information Technologies, JINR, 141980 Dubna, Russia*

¹²*Institute of Nuclear Physics, 050032 Almaty, Kazakhstan*

¹³*Nuclear Research Institute, 670000 Dalat, Vietnam*

¹⁴*AGH University of Science and Technology, Faculty of Physics and Applied Computer Science, 30-059 Krakow, Poland*

(Dated: June 27, 2024.)

Search for the population of the low-energy continuum of tetraneutron system was performed for reactions of the ^8He beam on deuterium target. These studies are performed for the data [I.A. Muzalevskii *et al.*, Phys. Rev. C **103**, 044313 (2021)], previously used for the studies of ^7H and ^6H in the $^2\text{H}(^8\text{He}, ^3\text{He})^7\text{H}$ and $^2\text{H}(^8\text{He}, ^4\text{He})^6\text{H}$ reactions. Evidence for a hump in the ^4n continuum at 3.5 ± 0.7 and 3.2 ± 0.8 MeV, was observed in the $^2\text{H}(^8\text{He}, ^6\text{Li})^4\text{n}$ and $^2\text{H}(^8\text{He}, ^3\text{He})^7\text{H} \rightarrow ^3\text{H} + ^4\text{n}$ reactions, respectively. The observed statistics is quite low (6 and up to 40 events) corresponding to very low cross sections of few microbarns or tens of microbarns. The background conditions for the $^2\text{H}(^8\text{He}, ^6\text{Li})^4\text{n}$ reaction are shown to be good, favoring the physical nature of the observed events. The $^2\text{H}(^8\text{He}, ^3\text{He})^7\text{H} \rightarrow ^3\text{H} + ^4\text{n}$ process transforms to the $^2\text{H}(^8\text{He}, ^6\text{Li}^*)^4\text{n}$ reaction in the limit of the highest ^7H decay energies. The population of the low-energy region in the ^4n spectrum is found to be perfectly correlated with the population of the lowest ^6Li states in the $^3\text{He} + ^3\text{H}$ continuum. Theoretical calculations of ^8He in a five-body $\alpha + 4\text{n}$ and of ^4n in a four-body hyperspherical models are presented. The ^8He wave function is shown to contain strong specific correlations, which may give rise to very low-energy structures in tetraneutron continuum in extreme-peripheral reaction scenarios.

I. INTRODUCTION

The search for the multineutron systems is old, but still unsettled problem of the low-energy nuclear physics. The first ideas about the possible multineutron systems stability were expressed in Refs. [1, 2] and since that time reiterated on various occasions. A detailed account of the multineutron studies history, both experimental and theoretical was provided in the recent review [3]. In short, either none or only marginal experimental evidence, which was never confirmed later, was obtained for the bound tetraneutron. However, such attempts continue, and there is a very recent example [4]. The situation has changed with the recent studies of ^4n population in reactions with ^8He , where four neutrons can be found in a spatially-separated neutron-halo configuration. In the $^4\text{He}(^8\text{He}, 2\alpha)$ reaction [5] 4 events were

observed in the low center-of-mass (c.m.) ^4n energy window $0 < E_T(4\text{n}) < 2$ MeV with the tiny cross section of ~ 4 nb. Even more recently, a statistically convincing peak (reported as “resonance-like structure”, ~ 44 events) was observed in a $^1\text{H}(^8\text{He}, p\alpha)$ experiment [6] at $E_T(4\text{n}) = 2.37$ MeV with $\Gamma = 1.75$ MeV. The reported cross section in this study is also small and estimated to be sub-microbarn. It should be noted that the both observations [5, 6] belong to the very specific situation of extreme backward (backward/forward in the case of [5]) kinematics of quasi-free scattering.

The issue of bound “multineutron nuclei” was scrutinized in the modern theoretical approaches [7–9] always with the same result: with fixed two-body potentials, radical modifications of the three-body potential are required. Such modifications are considered unacceptable as they are inconsistent with well-known nuclear structure. In the theoretical studies of the ^4n low-energy continuum various indications were found for important low-energy effect of the ^4n final-state interaction (FSI). These include: specific trajectories of the S -matrix poles,

* muzalevsky@jinr.ru

enhanced “time delay”, energy extrapolations of multi-neutron states confined in traps, etc., see e.g. [10–16] and, especially, the illuminating summary of those studies in [3]. There have been two works that, unlike those cited above, have predicted a 4n resonant state [17, 18], strongly contradicting the other studies.

An approach to 4n system tractable in terms of observables (namely, the reactions with neutron-rich halos) was presented in [19], wherein the 4n continuum is populated from the “prearranged” 4 neutron configurations in the “atmosphere” of a halo nucleus like ${}^8\text{He}$. The approach predicts population at low $E_T(4n)$ energies, but this population is a result of a specific (very peripheral) initial state structure (ISS) sampling, modified by FSI and should not be considered a stand-alone resonance. The formation of such a low-energy continuum response is partly analogous to the mechanism of the “soft dipole mode” formation in halo nuclei: (i) relatively very weak FSI effects and (ii) strong low-energy concentration of the strength function due to the peripheral character of the halo wave functions (WF) and the periphery enhancement by electromagnetic transition operators [20–22]. Principal message of [19] is that both halo character of ${}^8\text{He}$ WF and 4n FSI are not sufficient to produce low-energy response in the 4n continuum, additional peripheral assumption about reaction mechanism is required. In [23] the data of [6] were analyzed under assumptions similar to Ref. [19]. However, conclusion was made in [23] that the ${}^8\text{He}$ -induced source can directly explain the data of [6] without any peripheral assumptions. This is in a qualitative contradiction with the results of [19].

In this work we demonstrate that an evidence for the low-energy structures, analogous to the observations of [5, 6], can be found in the other reactions with the ${}^8\text{He}$ beam. As for the theoretical discussion, we revisit the 4n population from ${}^8\text{He}$ in simple approach [19] introducing important technical improvements. We generally confirm the results of [19], but provide an additional insight into the reaction mechanism, connected with specific correlations in the ${}^8\text{He}$ WF. Possible reasons for disagreement with the results of [23] are analyzed.

The system of units $\hbar = c = 1$ is used in this work.

II. EXPERIMENT

Experiments with the ${}^8\text{He}$ beam impinging on the deuterium target was performed at the ACCULINNA-2 facility (FLNR, JINR) having the search for the ${}^7\text{H}$ nuclide as a goal [24, 25]. The experiment appeared to be much “richer” than initially intended, providing interesting results also on ${}^6\text{H}$ [26] and other auxiliary channels like ${}^8\text{Li}$, ${}^9\text{Li}$ [27, 28] and ${}^5\text{H}$, ${}^5\text{He}$, ${}^7\text{He}$ [29]. Here we present the results obtained for the ${}^2\text{H}({}^8\text{He}, {}^6\text{Li}){}^4n$ and ${}^2\text{H}({}^8\text{He}, {}^3\text{He}){}^7\text{H} \rightarrow {}^3\text{H} + {}^4n$ reactions, previously omitted. Since the experiment has been already well presented in literature, we only briefly describe here the most relevant details.

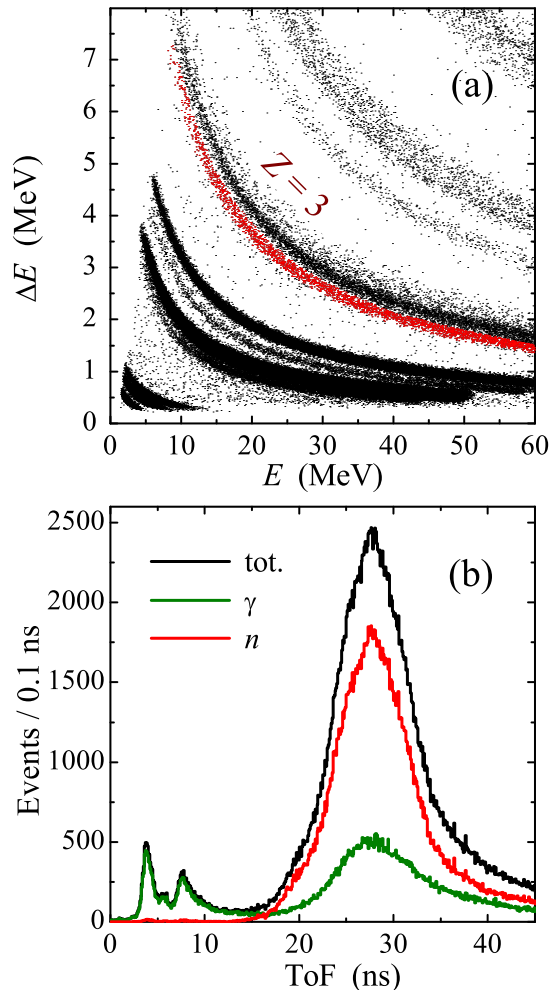


FIG. 1. (a) Identification of ${}^6\text{Li}$ recoil nuclei (red dots) by ΔE - E method in the side telescopes. (b) The ToF distribution obtained for the stilbene-array signals triggered by the side telescopes. The set of three peaks with ToF < 13 ns corresponds to the gamma rays produced in the diaphragm installed 20 cm upstream the target plane, in the target frame, and in CsI(Tl) array. The green and red histograms are formed by the events, identified by the ΔE -TAC method as gammas and neutrons, correspondingly.

The ${}^8\text{He}$ beam was produced at 26 A MeV with intensity $\approx 10^5$ pps. The beam was focused on the cryogenic gaseous deuterium target, with a temperature of 27 K, equipped with the thin stainless-steel and mylar windows. The target thickness was 3.7×10^{20} atoms \cdot cm $^{-2}$. For the ${}^2\text{H}({}^8\text{He}, {}^6\text{Li}){}^4n$ reaction the setup allowed us to measure the ${}^6\text{Li}$ recoil in coincidence with a neutron from the produced unbound 4n system.

The beam particles were identified by the two plastic scintillators, allowing to deduce the energy of the projectile from its measured time-of-flight (ToF). The projectile trajectories were reconstructed by the two pairs of multi-wire proportional chambers. The special run with the empty target cell was performed to estimate the back-

ground conditions, which had $\approx 16\%$ of the total ${}^8\text{He}$ beam time.

The recoil ${}^6\text{Li}$ nuclei, appearing in the ${}^2\text{H}({}^8\text{He}, {}^6\text{Li})$ reaction hit the array of four identical ΔE - E - E telescopes. The telescope array was located 179 mm downstream the target. Each telescope consisted of three layers of silicon strip detectors (SSDs). The 20- μm -thick SSD with a sensitive area of $50 \times 50 \text{ mm}^2$ was divided into 16 strips, the second and the third layers were created by the two identical 1 mm-thick SSDs ($60 \times 60 \text{ mm}^2$ with 16 strips). The ${}^6\text{Li}$ recoils emitted from the deuterium gas target in the ${}^2\text{H}({}^8\text{He}, {}^6\text{Li})$ reaction in a range 6 – 24 degrees in the lab system were detected by this telescope array. The telescopes allowed to identify ${}^6\text{Li}$ with clear separation from the other registered lithium isotopes, see Fig. 1 (a). The central telescope was installed at the beam line at the distance of 323 mm behind the target. It was intended to detect tritons emitted with high energies at the angles smaller than 9° in the laboratory system. The telescope consisted of one 1.5-mm-thick double-sided SSD ($64 \times 64 \text{ mm}^2$, with 32 strips on each side) followed by a square array of 16 CsI(Tl) crystals. The crystals had a cross section of $16.5 \times 16.5 \text{ mm}^2$ and thickness 50 mm each.

The group of four neutrons appears in “free flight” as a result of the α -core removal from the ${}^8\text{He}$ projectile. An important part of the ${}^2\text{H}({}^8\text{He}, {}^6\text{Li}){}^4\text{n}$ reaction analysis was the neutron identification and reconstruction. The neutron-wall setup [30] included 48 stilbene scintillator crystals placed on a $0.7 \times 1.1 \text{ m}^2$ area located 2 m downstream the target at zero angle to the beam axis. The distance between the 50-mm thick and 80-mm diameter stilbene crystals was approximately 12 cm which resulted in about 30% probability for neutrons to hit a stilbene detector. The stilbene array provided 4.5% energy resolution and the single neutron registration efficiency of $\approx 1\%$. The probability of a neutron registration in coincidence with the ${}^6\text{Li}$ recoil was around 3%, taking into account that four neutrons are flying forward, towards the stilbene array. The n -gamma separation was made by means of the Pulse Shape Discrimination (PSD) [30]. The PSD information, supplemented with ToF distribution, see Fig. 1 (b), leads to suggestion that some gamma-type signals correspond to neutron-like ToF. These gammas are presumably produced by neutrons interacting with the stilbene modules housings and should be taken as neutron events.

A. ${}^2\text{H}({}^8\text{He}, {}^6\text{Li}){}^4\text{n}$ results

Tetraneutron was reconstructed from the recoil ${}^6\text{Li}$ as a missing-mass (MM) component in the ${}^2\text{H}({}^8\text{He}, {}^6\text{Li})$ reaction. The total number of ${}^6\text{Li}$ - n coincidences found in the recorded data was 136, see Fig. 2 (a). In this figure the neutron kinetic energy E_n in the ${}^4\text{n}$ c.m. frame is compared with the reconstructed MM energy $E_T(4n)$ of the ${}^4\text{n}$ group. The fact that the majority of these events (108 events) are located inside the kinematically allowed

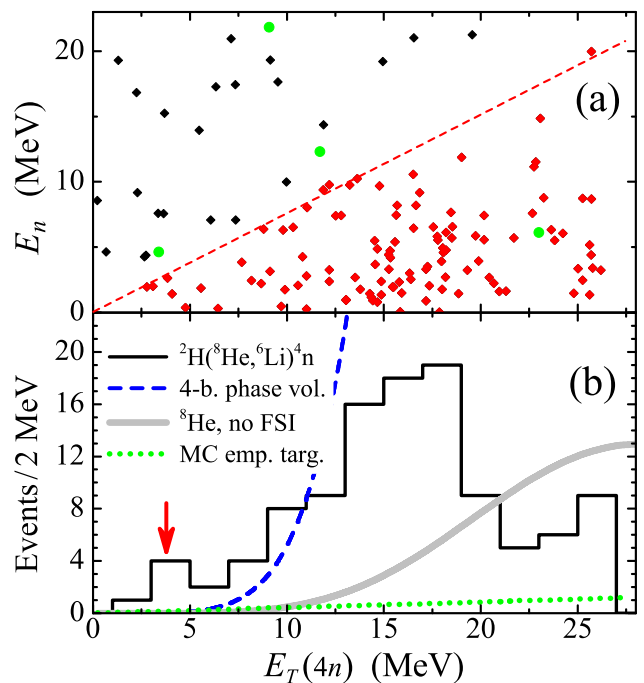


FIG. 2. (a) Correlation between the neutron energy in the ${}^4\text{n}$ frame and the ${}^4\text{n}$ decay energy for the ${}^2\text{H}({}^8\text{He}, {}^6\text{Li}){}^4\text{n}$ reaction. The kinematical limit $E_n < 3E_T(4n)/4$ is shown by the red dashed line separating the accepted events (red diamonds) and rejected events (black diamonds). The empty-target measurement events are shown by large green circles. (b) The ${}^4\text{n}$ MM spectrum. Green dotted curve shows the simulated empty-target spectrum assuming the uniform distribution of background events in the $\{E_T(4n), E_n\}$ kinematical plane. The blue dashed curve corresponds to the 4-body phase volume $\sim E_T^{11/2}$ and thick gray curve to Fourier transform of the ${}^8\text{He}$ source.

region proves a good channel identification for the data. The empty-target measurement Fig. 2 (a) shows that the background conditions were very “clean” for the ${}^4\text{n}$ population in the ${}^2\text{H}({}^8\text{He}, {}^6\text{Li})$ reaction: the empty-target events are very few and located mainly in the unphysical part of the kinematical plane.

The MM spectrum of ${}^4\text{n}$, Fig. 2 (b), was reconstructed from the measured ${}^6\text{Li}$ recoil energy and emission angle, taking the 108 events located within the “kinematical triangle” $E_n < 3E_T(4n)/4$. The obtained spectrum shows a group of 6 events around $E_T(4n) \approx 3.5 \text{ MeV}$. The width of this group is well consistent with the value of energy resolution $\sim 2 \text{ MeV}$ FWHM in this region of ${}^4\text{n}$ MM spectrum. The statistics of this low-energy group is quite low, but the energy resolution is sufficient and the background conditions are shown above to be very good. The green dotted curve Fig. 2 (b) shows the Monte Carlo (MC) simulated empty-target contribution. It can be seen that less than 1 random event is expected under $E_T(4n) = 6 \text{ MeV}$. Then the Poisson probability to get 6 random coincidences in that energy region is then $\lesssim 0.05\%$.

Obviously, the observed low-energy hump in Fig. 2 (b)

can not be described just as a contribution of the 4-body phase volume or Fourier transform of the ^8He source, see also Fig. 8 (d) and the related discussion in Sec. VI. The phase volume for uncorrelated decay of A -body system, which can be regarded here as minimal admissible model, is

$$\frac{dW}{dE_T(A)} \propto E_T^{(3A-5)/2}(A), \quad (1)$$

and the generic 4-body phase volume behavior is $\sim E_T^{7/2}$. However, Eq. (1) should be modified by the minimum number of excitation quanta n_{\min} allowed for the continuum WF as

$$\frac{dW}{dE_T(A)} \propto E_T^{(3A-5)/2+n_{\min}}(A). \quad (2)$$

For the ^4n system the Pauli principle requires two additional excitation quanta for the 0^+ lowest-energy configuration. This corresponds to $[s^2p^2]_0$ lowest-energy configuration in the shell-model terms or to $n_{\min} = K_{\min} = 2$ in terms of the hyperspherical harmonics (HH) model principal quantum number K , see Section IV. This leads to a modified 4-body phase-volume behavior $\sim E_T^{11/2}$ shown in Fig. 2 (b).

It is notable that the observed energy of this group of events $3.5 \pm 0.35(\text{stat.}) \pm 0.6(\text{sys.})$ MeV is consistent within the experimental energy resolution with the ^4n low-energy peak value $2.37 \pm 0.38(\text{stat.}) \pm 0.44(\text{sys.})$ MeV reported in Ref. [6].

The $^2\text{H}(^8\text{He}, ^6\text{Li})^4\text{n}$ reaction has already been used before for tetra-neutron search, but the results were not published in details [31, 32]. Rather low statistics resonant-like structure was reported in [31] for the ^4n missing mass spectrum at 2.5 MeV above threshold. In contrast, in analogous experimental run [32] the ^4n spectrum with $E_T(^4\text{n}) \lesssim 5$ MeV was found to be dominated by the carbon background due to the use of the CD_2 target. As compared to studies of [31, 32] our experiment has no carbon background and additional background elimination connected with kinematics of Fig. 2 (a) is possible.

B. $^2\text{H}(^8\text{He}, ^3\text{He})^7\text{H} \rightarrow ^3\text{H} + ^4\text{n}$ results

In Ref. [25] the excitation spectrum of ^7H was populated in the $^2\text{H}(^8\text{He}, ^3\text{He})^7\text{H}$ reaction up to $E_T(^7\text{H}) \sim 17$ MeV above the 5-body $^3\text{H} + 4\text{n}$ decay threshold. An evidence was reported for resonant states at $E_T(^7\text{H}) = 2.2(5)$ and $5.5(3)$ MeV and also some indications for such states at $7.5(3)$ and $11.0(3)$ MeV. These structures were observed at small c.m. reaction angles $\theta_{\text{c.m.}} < 18^\circ$. The ^7H excitations in a broad range $\theta_{\text{c.m.}} < 43^\circ$ with $E_T(^7\text{H}) > 6$ MeV form quite a featureless hump up to maximal available energy. It is possible to search for the low-energy-correlated ^4n emission off these sufficiently highly-excited configurations of ^7H .

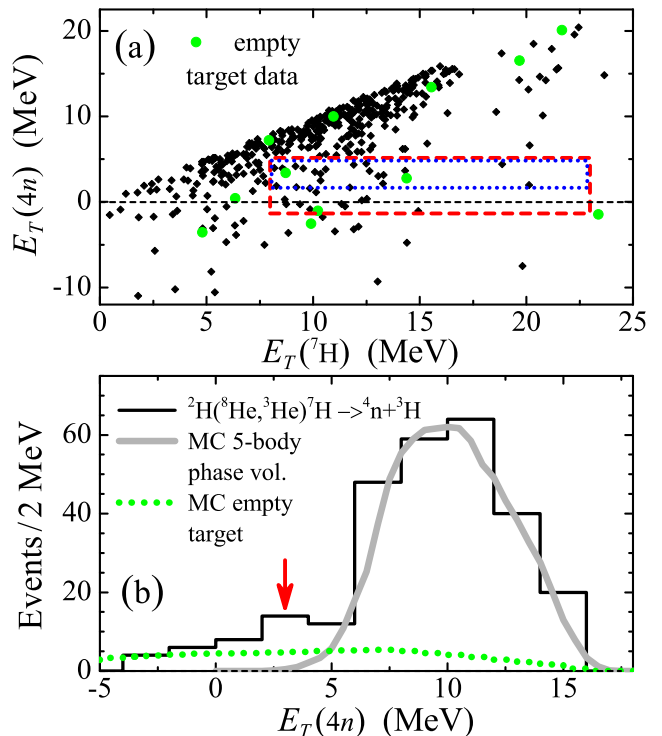


FIG. 3. (a) “Kinematical triangle” for ^4n MM vs. ^7H MM for the $^2\text{H}(^8\text{He}, ^3\text{He})^7\text{H}$ data of [25]. Large green circles show the empty target events. Red dashed and blue dotted frames show the event selection for Fig. 4 (b). (b) Tetra-neutron MM spectrum summed up for $E_T(^7\text{H}) > 8$ MeV. Green dotted curve shows the simulated empty-target spectrum assuming the uniform distribution of background events in the $\{E_T(^7\text{H}), E_T(^4\text{n})\}$ kinematical plane. Thick gray line is MC simulated phase volume for ^7H decays.

The data of Ref. [25] contain coincidence information on the ^3H decay product of ^7H , which allows one to infer the MM of the ^4n subsystem. These data in terms of the ^4n emission are shown in Fig. 3 (a). The ^7H events are mainly concentrated close to diagonal $E_T(^4\text{n}) = E_T(^7\text{H})$, which means that the “internal” energy of the tetra-neutron tends to be large, while the triton gets only a small fraction of the total ^7H decay energy. This situation is close to the phase-volume distribution of the 5-body $^3\text{H} + 4\text{n}$ decay for the given ^7H decay energy $E_T(^7\text{H})$ as

$$\frac{dW}{dE_T(^7\text{H}) d\varepsilon} \propto E_T^{\alpha+3/2}(^7\text{H}) \sqrt{\varepsilon^\alpha(1-\varepsilon)}, \quad (3)$$

in terms of ^4n energy-distribution parameter

$$\varepsilon = E_T(^4\text{n})/E_T(^7\text{H}).$$

The standard value for the 5-body phase volume is $\alpha = 7$. Eq. (3) is the double-differential form of the Eq. (2), discussed in the previous Section, so it can be found that at least $\alpha = 11$ value is requested for $\varepsilon \rightarrow 0$ by the Pauli principle for ^4n . This idea is confirmed by the calcula-

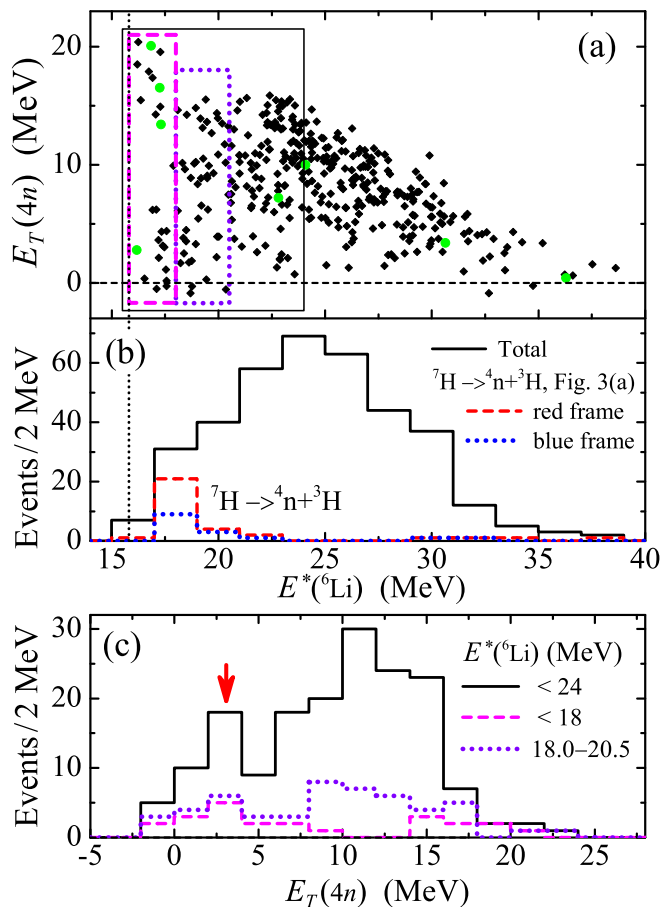


FIG. 4. (a) “Kinematical triangle” for ${}^4\text{n}$ MM vs. $E^*({}^6\text{Li})$ MM for the ${}^2\text{H}({}^8\text{He}, {}^3\text{He}){}^7\text{H}$ data of [25]. Large green circles show the empty target events. (b) ${}^6\text{Li}^*$ MM spectrum (black solid histogram). Red dashed and blue dotted histograms show spectra corresponding to selection frames in Fig. 3 (a). The vertical dotted line in panels (a) and (b) indicate the ${}^3\text{He}+{}^3\text{H}$ threshold at $E^*({}^6\text{Li})=15.8$ MeV. (c) Tetra-neutron MM spectrum gated on the lowest states in the ${}^3\text{He}+{}^3\text{H}$ continuum of the ${}^6\text{Li}^*$ system, see frames of corresponding style in the panel (a).

tions of the 5-body decay of ${}^7\text{H}$ in [33]. The ε distributions at given ${}^7\text{H}$ energies are also quite “compressed” due to the experimental bias, see Fig. 13 of [25], so $\alpha = 11$ for the distribution of Eq. (3) turns out to be completely justified in our situation.

To observe a possible ${}^4\text{n}$ correlation, we need to find the kinematical region, where the main “phase-volume” component of the decay distribution Eq. (3) is well suppressed. This means $\varepsilon \lesssim 0.5$, and for the studies of the ${}^4\text{n}$ excitation region $E_T({}^4\text{n}) \sim 2-4$ MeV we need to consider the ${}^7\text{H}$ decay energy region $E_T({}^7\text{H}) > 8$ MeV. Under this selection condition, the hump with $E_T({}^4\text{n}) \sim 2-4$ MeV can be found in the ${}^4\text{n}$ MM spectrum, see Fig. 3 (b). The MC simulated phase volume only weakly “penetrates” in the $E_T({}^4\text{n}) \sim 2-4$ MeV region. The background of

about 2–3 events/MeV is estimated from the available empty target data, see green circles in Fig. 3 (b). Thus a significant part of this low-energy ${}^4\text{n}$ data *may be* connected (but not necessarily *is connected*, as we see below) with the random background.

The ${}^7\text{H}$ data can be converted to presentation of ${}^6\text{Li}^*$ system reconstructed as ${}^3\text{He}+{}^3\text{H}$ continuum, see Fig. 4 (a). Fortunately, it appeared that the low-energy ${}^4\text{n}$ events in Fig. 3 (b) are practically perfectly correlated with the population of the lowest ${}^6\text{Li}^*$ state in the ${}^3\text{He}+{}^3\text{H}$ continuum, with $E^*({}^6\text{Li}) \sim 18$ MeV and $\Gamma \sim 3$ MeV [34], see Fig. 4 (b). This means that we are actually dealing here not with the ${}^7\text{H} \rightarrow {}^3\text{H}+{}^4\text{n}$ decay, but rather with the ${}^2\text{H}({}^8\text{He}, {}^6\text{Li}^*){}^4\text{n}$ reaction. Moreover, the same correlation is perfectly true not only for events in the $E_T({}^4\text{n}) \sim 2-5$ MeV range, but also for the $-1.5 < E_T({}^4\text{n}) < 2$ MeV range. In this range most of the events should be either unphysical or connected with insufficient energy resolution, as the population of the $E_T({}^4\text{n}) \lesssim 1$ MeV range is predicted to be negligible in available theoretical scenarios, see Fig. 7 or Ref. [23]. The MC estimated energy resolution for the ${}^4\text{n}$ MM spectrum is ~ 2.5 MeV FWHM. However, this resolution has a broad “nongaussian” component, which may result in some number of events with $E_T({}^4\text{n}) \sim -1$ MeV. The coincidence with the definite state in ${}^6\text{Li}$ practically guarantee the physical nature of such event, so we recognize that the absolute majority of events (26 out of 28) found in the range $-1.5 < E_T({}^4\text{n}) < 5$ MeV in Fig. 3 (b) as really belonging to the ${}^4\text{n}$ MM spectrum.

Strong correlation found in Fig. 4 (b) inspired us to “reverse” the logic and construct the ${}^4\text{n}$ spectrum gated by the lowest states in the ${}^6\text{Li}^*$ continuum, see Fig. 4 (c). The profile of the low-energy $E_T({}^4\text{n}) < 6$ MeV ${}^4\text{n}$ spectrum is practically insensitive to the ${}^6\text{Li}^*$ gate energy selection for $E^*({}^6\text{Li}) < 24$ MeV. For higher $E^*({}^6\text{Li})$ energies the ${}^4\text{n}$ spectrum expectedly becomes phase-volume-like. The peak energy can be found as $3.2 \pm 0.45(\text{stat.}) \pm 0.7(\text{sys.})$ MeV. That peak position is consistent with $2.37 \pm 0.38(\text{stat.}) \pm 0.44(\text{sys.})$ MeV of Ref. [6] within the experimental energy resolution. Statistically our data is analogous to data [6]: 44 events in [6] vs. 26 and 40 events in the ≤ 20.5 and ≤ 24 MeV $E^*({}^6\text{Li})$ gates, respectively.

There is a strong sensitivity of the obtained ${}^4\text{n}$ MM spectrum to the energy of the populated ${}^6\text{Li}$ states. For example, it can be seen in Fig. 4 (c) that ${}^4\text{n}$ spectra in the $E^*({}^6\text{Li})$ gates $\{15.8, 18\}$ and $\{18, 20.5\}$ MeV show populations 4 events versus 25 events in the $8 < E_T({}^4\text{n}) < 16$ MeV range, which seem to be beyond statistical uncertainty. This may be indication that mechanisms for ${}^4\text{n}$ population within these gates are somewhat different: the states of the ${}^6\text{Li}$ recoil are broad and overlapping in this energy range [34], and the higher-energy $E^*({}^6\text{Li})$ gate could be “contaminated” by contributions of the higher excitations of ${}^6\text{Li}$.

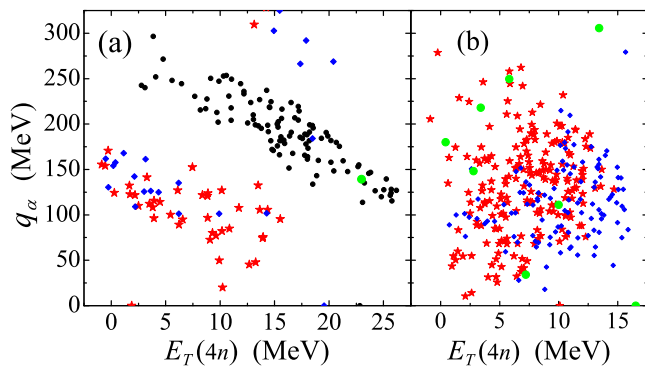


FIG. 5. Momentum transfer to ${}^4\text{n}$ system for the ${}^2\text{H}({}^8\text{He}, {}^6\text{Li}){}^4\text{n}$ reaction is shown by black circles in (a). The same for the ${}^2\text{H}({}^8\text{He}, {}^3\text{He}){}^7\text{H} \rightarrow {}^3\text{H} + {}^4\text{n}$ reaction: blue diamonds and red stars in (a) correspond to $E^*({}^6\text{Li})$ ranges $\{15.8, 18\}$ and $\{18, 20.5\}$ MeV, blue diamonds and red stars in (b) correspond to $\{20.5, 24\}$ and $\{24, 40\}$ MeV. Large green circles show the corresponding empty target events.

III. ON TETRANEUTRON POPULATION IN DIFFERENT REACTIONS

The low-energy population of ${}^4\text{n}$ in [6] and in the processes considered in this work all have the ${}^8\text{He}$ nuclide as a starting point. At first glance, this is the only similarity, and the reaction mechanisms should be too different. Let’s demonstrate that the differences are actually not so striking.

Table I shows the momenta and velocities in the recoil-product channel for the reaction of Ref. [6] and the reactions considered in this work. Of course, in the reaction of [6] the “recoil” particles are leaving the FSI region faster, than in the case of our $(d, {}^6\text{Li})$ reaction, but in the timescale this “faster” is only a factor of 2.

The ${}^2\text{H}({}^8\text{He}, {}^3\text{He}){}^7\text{H} \rightarrow {}^3\text{H} + {}^4\text{n}$ process formally has the decay process as the second step. In fact, from Table I it is clear that for the excited states of ${}^7\text{H}$, which we consider, the velocity of the ${}^3\text{H}$ recoil leaving ${}^4\text{n}$ in the “decay process” is actually comparable with the velocity, at which the ${}^3\text{He}$ recoil had left the FSI region in the first [the ${}^2\text{H}({}^8\text{He}, {}^3\text{He}){}^7\text{H}$ reaction] step of this process. This kinematical region is actually a transition region from ${}^2\text{H}({}^8\text{He}, {}^3\text{He}){}^7\text{H}$ reaction to ${}^2\text{H}({}^8\text{He}, {}^6\text{Li}^*){}^4\text{n}$, where

TABLE I. Relative momentum K' and relative velocities v' in the recoil-product channel for reactions of interest.

Reaction	Recoil	K' (MeV)	v'
${}^1\text{H}({}^8\text{He}, p\alpha){}^4\text{n}$, Ref. [6]	${}^5\text{Li}$	750	0.36
${}^2\text{H}({}^8\text{He}, {}^6\text{Li}){}^4\text{n}$	${}^6\text{Li}$	426	0.19
${}^2\text{H}({}^8\text{He}, {}^3\text{He}){}^7\text{H}$	${}^3\text{He}$	311	0.16
${}^7\text{H} \rightarrow {}^3\text{H} + {}^4\text{n}$	${}^3\text{H}$	120 – 200	0.08 – 0.13

highly excited states of ${}^6\text{Li}$ (those located above the ${}^3\text{He}-{}^3\text{H}$ threshold) are populated. We find in Fig. 4 (c) that the most expressed low-energy ${}^4\text{n}$ hump not “contaminated” with higher-energy phase-volume-like contributions is obtained for the ${}^6\text{Li}^*$ recoil, which is the lowest ${}^3\text{He}-{}^3\text{H}$ resonant state.

So, we see that the low-energy ${}^4\text{n}$ continuum is confidently populated in the ${}^2\text{H}({}^8\text{He}, {}^6\text{Li}^*){}^4\text{n}$ reactions with excitation energies $E^*({}^6\text{Li}) = 0$ MeV, see Fig. 2 (b), and $E^*({}^6\text{Li}) \sim 18$ MeV, see Fig. 4 (c). It is quite natural to expect that such a population should also take place at the intermediate energies, which corresponds to $\alpha+d$ continuum states of ${}^6\text{Li}$. These would be reactions of quasifree scattering ${}^2\text{H}({}^8\text{He}, d\alpha){}^4\text{n}$, which have never considered seriously because of extremely “soft” ${}^2\text{H}$ target. So far, the possibility to extract this information from our existing data is questionable.

Another characteristic, which is expectedly very important for the direct reactions, is momentum transfer to the ${}^4\text{n}$ system q_α , see also the Eq. (9). For our reactions the q_α values are easily reconstructed, see Fig. 5. The momentum transfers $q_\alpha \sim 130$ and $q_\alpha \sim 270$ MeV are realized for the low-energy ${}^4\text{n}$ population in the ${}^2\text{H}({}^8\text{He}, {}^6\text{Li}){}^4\text{n}$ and ${}^2\text{H}({}^8\text{He}, {}^3\text{He}){}^7\text{H} \rightarrow {}^3\text{H} + {}^4\text{n}$ reactions, respectively. This is found important for data interpretation, see Fig. 7 and related text. Unfortunately, we do not find information on the momentum transfers in Ref. [6], though this information is obviously accessible in these data. Only the restriction $0 < q_\alpha < 250$ MeV can be roughly estimated from Fig. 2 of [6], while the most probable value seem to be around $q_\alpha \sim 60$ MeV.

IV. THEORETICAL MODEL

In this work we performed studies of ${}^8\text{He}$ in a five-body $\alpha+4n$ and of ${}^4\text{n}$ in a four-body hyperspherical harmonics models. A detailed description of these studies will be given elsewhere, while here we focus on the aspects related to ${}^4\text{n}$ production from ${}^8\text{He}$, following the ideology of Ref. [19]. The HH Schrödinger equation (SE) for A particles is used either without (bound states) or with right-hand-side inhomogeneity (continuum states):

$$\left(\hat{H}_A - E_T\right) \Psi_A^{(b,+)} = F_{\mathbf{q}}. \quad (4)$$

On the properly antisymmetrized HH basis $\mathcal{J}_{K\gamma}(\Omega_\rho)$ the variational procedure reduces the SE with inhomogeneous term (4) to a set of coupled ordinary differential

TABLE II. Geometry of ${}^8\text{He}$ (rms radial characteristics in fm) versus experimental data.

	$\langle r_{nn} \rangle$	$\langle r_{\alpha n} \rangle$	$\langle r_\alpha \rangle$	$\langle r_n \rangle$	R_{mat}	R_{ch}
Th.	4.15	3.34	1.06	2.72	2.34	1.96
Exp.				2.71(7)	2.48(3)	1.956(16)

equations:

$$\begin{aligned} \Psi_A^{(b,+)}(\rho, \Omega_\rho) &= \rho^{-N_A} \sum_{K\gamma} \chi_{K\gamma}^{(b,+)}(\rho) \mathcal{J}_{K\gamma}^\dagger(\Omega_\rho), \\ \left[\frac{d^2}{d\rho^2} - \frac{\mathcal{L}(\mathcal{L}+1)}{\rho^2} + 2M \{E_T - V_{K\gamma, K\gamma}(\rho)\} \right] \chi_{K\gamma}(\rho) \\ &= \sum_{K'\gamma'} 2M V_{K\gamma, K'\gamma'}(\rho) \chi_{K'\gamma'}(\rho) + f_{\mathbf{q}, K\gamma}(\rho), \end{aligned} \quad (5)$$

$$\begin{aligned} V_{K\gamma, K'\gamma'}(\rho) &= \int d\Omega_\rho \mathcal{J}_{K\gamma}^\dagger(\Omega_\rho) [V_2 + V_3] \mathcal{J}_{K'\gamma'}(\Omega_\rho), \quad (6) \\ V_2 &= \sum_{i>j} \hat{V}(\mathbf{r}_{ij}), \quad V_3 = \sum_{i>j>k} \hat{V}(\mathbf{r}_{ij}, \mathbf{r}_{jk}), \end{aligned}$$

where $\hat{V}(\mathbf{r}_{ij})$ are two-body potentials $V_{2N}(\mathbf{r}_{ij})$ or $V_{\text{Core-}N}(\mathbf{r}_{ij})$, while $\hat{V}(\mathbf{r}_{ij}, \mathbf{r}_{jk})$ are three-body potentials $V_{3N}(\mathbf{r}_{ij}, \mathbf{r}_{jk})$ or $V_{\text{Core-}NN}(\mathbf{r}_{ij}, \mathbf{r}_{jk})$. The ‘‘multiindex’’ $\{K\gamma\}$ is numbering the available HH basis states. The hypermomentum K is the grand quantum number in the few-body configuration space and

$$\mathcal{L} = K + (3A - 6)/2, \quad N_A = (3A - 4)/2.$$

For ${}^8\text{He}$ and ${}^4\text{n}$ its minimum value is $K_{\min} = 2$ due to the Pauli principle for four neutrons.

For the SE (5) without Coulomb interaction the boundary conditions at large ρ are known analytically

$$\begin{aligned} \chi_{K\gamma}^{(b)}(\rho) &\sim \sqrt{2\kappa\rho/\pi} \mathcal{K}_{\mathcal{L}+1/2}(\kappa\rho) \sim \exp[-\kappa\rho], \\ \chi_{K\gamma}^{(+)}(\rho) &\sim \mathcal{H}_{\mathcal{L}}^{(+)}(\kappa\rho) \sim \exp[+i\kappa\rho], \end{aligned} \quad (7)$$

where $\kappa = \sqrt{2M|E_T|}$, \mathcal{K} are the modified Bessel functions of the second kind, $\mathcal{H}^{(+)}$ are the Riccati-Bessel functions.

The ‘‘source functions’’ $f_{\mathbf{q}, K\gamma}(\rho)$ are terms of hyperspherical expansion of the inhomogeneous term $F_{\mathbf{q}}$:

$$f_{\mathbf{q}, K\gamma}(\rho) = \rho^{N_A} \int d\Omega_\rho \mathcal{J}_{K\gamma}^\dagger(\Omega_\rho) F_{\mathbf{q}}(\rho, \Omega_\rho). \quad (8)$$

The simplest reaction model which can be considered for ${}^4\text{n}$ production is ‘‘sudden removal’’ of core from ${}^8\text{He}$ [19, 23]. This procedure defines the source function $F_{\mathbf{q}}$ in (4) as the Fourier transform of the overlap integral of the α -cluster WF Ψ_α and the ${}^8\text{He}$ WF over the radius-vector \mathbf{r}_α between the removed α -cluster and the ${}^4\text{n}$ center-of-mass:

$$F_{\mathbf{q}\alpha} = \int d^3r_\alpha e^{i\mathbf{q}\alpha\mathbf{r}_\alpha} \langle \Psi_\alpha | \Psi_{s\text{He}} \rangle. \quad (9)$$

The ‘‘strength function’’ for population of the ${}^4\text{n}$ continuum should be proportional to the outgoing flux of A particles, expressed via the WFs with pure outgoing wave boundary conditions Eq. (7)

$$\frac{dW}{dE_T} \sim j = \frac{1}{M} \text{Im} \int d\Omega_\rho \Psi_A^{(+)\dagger} \rho^{N_A} \frac{d}{d\rho} \rho^{N_A} \Psi_A^{(+)} \Big|_{\rho=\rho_{\max}}, \quad (10)$$

on a hypersphere of a large radius $\rho_{\max} \sim 300 - 500$ fm.

V. PROPERTIES OF THE ${}^8\text{He}$

Following the cluster $\alpha+n+n$ model studies of ${}^6\text{He}$, ${}^6\text{Li}$, ${}^6\text{Be}$ isobar [22, 35, 36] we use the Sack-Biedenharn-Breit (SBB) potential [37] in the α - n channel. We suppress the Pauli forbidden state by using the additional repulsive core in s -wave potential, which provides practically the same scattering phases as the deep potential.

In the calculations we adopted the local charge independent Argonne SSC AV14 NN potential [40]. For evaluations we also used simple s -wave singlet NN potential Brown-Jackson (BJ) from [41]: $V_{2N}(r) = V_0 \exp[-r/r_0]$, $V_0 = -31$ MeV, $r_0 = 1.8$ fm. For three nucleons with separations r_{ij} we use the three-nucleon potential [42]

$$V_{3N} = \sum_{n=1,2} U_n \sum_{i>j>k} \exp[-\mu_n(r_{ij}^2 + r_{jk}^2 + r_{ki}^2)], \quad (11)$$

in Eq. (6). A set of the parameters $U_1 = -2.04$ MeV, $\mu_1 = (4.0 \text{ fm})^{-2}$, $U_2 = 35.0$ MeV, $\mu_2 = (0.75 \text{ fm})^{-2}$ yields the binding energies 8.41 (8.48), 7.74 (7.72), and 28.44 (28.30) MeV for ${}^3\text{H}$, ${}^3\text{He}$, and ${}^4\text{He}$ ground states, respectively (the experimental values are shown in parentheses).

We also adjusted the ${}^4\text{He}$ - n - n three-body potential of the same form as Eq. (11) to reproduce the ground state properties of ${}^6\text{He}$, which is well described in terms of the three-body ${}^4\text{He}$ - n - n model [22, 35, 36]. For ${}^8\text{He}$ g.s. the calculations were performed with $K_{\max} = 10$, containing 15862 basis states which are reduced to 675 states in (5) by antisymmetrization. The ${}^8\text{He}$ is slightly underbound (by approximately 115 KeV). This means some overbinding at higher K , but this does not matter for the study of the tetra-neutron: the geometry of the ${}^8\text{He}$ g.s. WF is much more important here. The percentages of the major ${}^8\text{He}$ WF components $\{^1S, ^3P\} = \{73, 27\}$ are in a good agreement with advanced *ab initio* Quantum Monte Carlo calculations of [43] $\{71, 29\}$ and [44] $\{63, 37\}$. The geometric characteristics of ${}^8\text{He}$ are compared with experimental data in the Table II. The root mean square (rms) charge radius R_{ch} of ${}^8\text{He}$, has been determined for the first time as 1.93(3) fm [45]. However, using the new charge radius 1.67824(83) fm of ${}^4\text{He}$ [46] as an anchor point for the isotope shift measurements, the ${}^8\text{He}$ charge radius was reevaluated as 1.9559(7)(158) fm, where the first uncertainty is from new charge radius value and the second uncertainty from the electronic isotope shift measurements. Our result for ${}^8\text{He}$ charge radius is in nice agreement with both experiments. The comparison with

TABLE III. Elastic and reaction cross sections for ${}^8\text{He}$ (in mb).

Reaction	${}^8\text{He-p}$, σ_{el}	${}^8\text{He-p}$, σ_r	${}^8\text{He-}{}^{12}\text{C}$, σ_r
Th.	51.6	196.6	807
Exp.	54.1(17) [38]	197.8(35) [38]	817(6) [39]

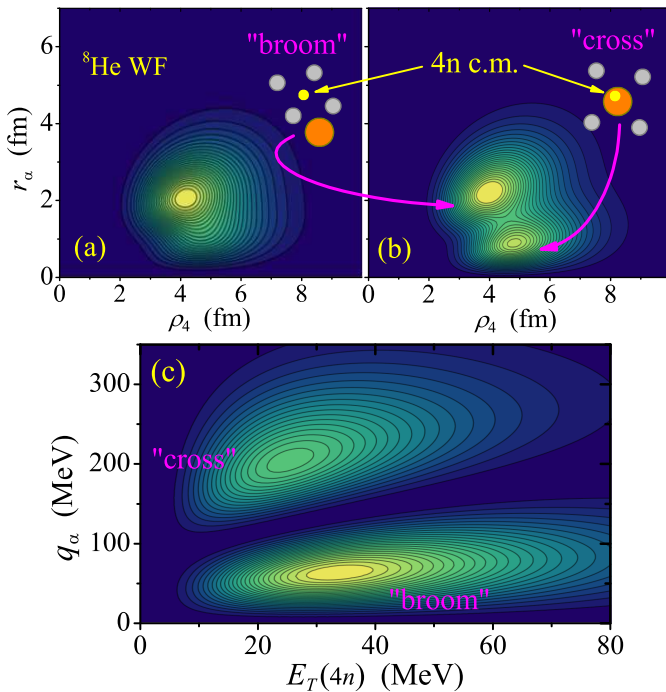


FIG. 6. (a) Correlation density of the ${}^8\text{He}$ WF. (b) Correlation density of the 0^+ ${}^4\text{n}$ source component with $L_\alpha = 0$ with qualitative illustrations of dominant correlation patterns. (c) Momentum-space correlations for dominant $K = 2$, $S = 0$ component of the source (b).

experimental rms matter radius R_{mat} in Table II, seems to be not so favorable, but we need to recall that this value is actually extracted from the high-energy reaction data in a model-dependent way. Therefore, here the direct comparison of cross sections is more preferable. The results of Glauber-like calculations with ${}^8\text{He}$ densities obtained in our model, shown in the Table III, are in a very good agreement with experimental data, including the cross section on the ${}^{12}\text{C}$ target [39], from which the matter radius of 2.48(3) fm, shown in Table II was actually extracted. Thus, we can expect that our ${}^8\text{He}$ WF, which near perfectly describes all known experimental data and reveals extremely important α - ${}^4\text{n}$ correlations is a reliable starting point for the tetra-neutron study.

VI. THE ${}^8\text{He}$ WF AS A SOURCE FOR TETRANEUTRON POPULATION

The ${}^8\text{He}$ WF correlation density r_α vs. ρ_4 (informative for the ${}^4\text{n}$ studies) is shown in Fig. 6 (a). It looks overall quite featureless. In contrast, the projection of the ${}^8\text{He}$ WF on the ${}^4\text{n}$ 0^+ configuration with $L_\alpha = 0$, where strongest ${}^4\text{n}$ FSI effect is expected, exhibits strong spatial correlations, see Fig. 6 (b). The correlation density r_α vs. ρ_4 can be easier perceived basing on a simple relation between the rms radius r_n of individual neutron

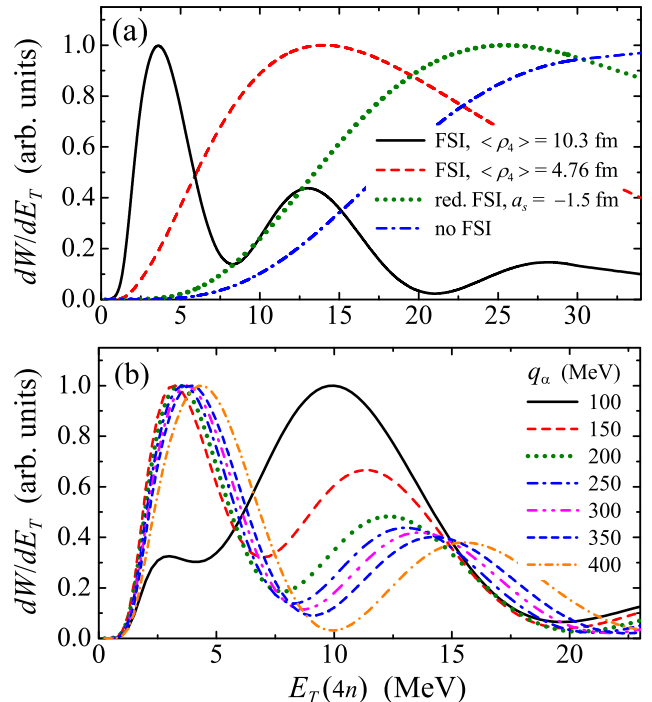


FIG. 7. (a) The ${}^4\text{n}$ spectra obtained for $q_\alpha = 250$ MeV without FSI, with reduced n - n FSI ($a_s = -1.5$ fm), full ${}^4\text{n}$ FSI with normal source and with peripheral source (black solid curve). (b) ${}^4\text{n}$ spectra obtained for different transferred momenta q_α for peripheral source.

in the ${}^4\text{n}$ c.m. frame and the ${}^4\text{n}$ rms hyperradius

$$\langle r_n \rangle = \langle \rho_4 \rangle / 2.$$

Following the well-known naming of spatial correlations in the classical ${}^6\text{He}$ halo nucleus — “dineutron” and “cigar” [35] — we characterize correlations in ${}^8\text{He}$ source as “broom” (compact tetra-neutron aside of α -particle) and “cross” (neutrons evenly distributed around central-located α -particle). The double-hump picture of correlations can be qualitatively understood as connected with $[s^2p^2]_0$ configuration (in the shell model notations) in analogy with $[p^2]_0$ configuration providing strong spatial focusing (“Pauli focusing” [35]) in the ${}^6\text{He}$ case. Fig. 6 (c) shows the Fourier transform of the source (b), illustrating the momentum content of this structure without ${}^4\text{n}$ FSI. So far, the Pauli focusing for the ${}^8\text{He}$ g.s. WF has been several times discussed in the qualitative models [33, 47, 48], but has never been demonstrated in the realistic calculations of the ${}^8\text{He}$ g.s. WF.

It should be understood that the strongly correlated source shown in Fig. 6 (b) is related to about 30% of the ${}^8\text{He}$ g.s. WF. The other components of these WF projected on ${}^4\text{n}$ system populate “excited” configurations of ${}^4\text{n}$, where we do not expect any strong final-state effect.

Figure 7 (a) shows the evolution of ${}^4\text{n}$ strength functions for selected $q_\alpha = 250$ MeV: no FSI \rightarrow reduced ${}^4\text{n}$ FSI \rightarrow full ${}^4\text{n}$ FSI. The strength function peak for full ${}^4\text{n}$

FSI is at about 14 MeV in a good agreement with analogous calculation in [19]. To form extreme low-energy peak in the strength function in the region 2.5 – 3.5 MeV as indicated by data, a further qualitative assumption of the peripheral character of reaction is needed. To evaluate it, we cut out small hyperradii of the original source function by a profile function of the form

$$f_{\mathbf{q},K\gamma}(\rho_4) \rightarrow \frac{f_{\mathbf{q},K\gamma}(\rho_4)}{1 + \exp[(\rho_{4f} - \rho_4)/d_{4f}]}, \quad (12)$$

and further refer it as “peripheral source”. With $\rho_{4f} = 10$ fm and $d_{4f} = 0.3$ fm the rms size of the source is increased to $\langle \rho_4 \rangle \sim 10$ fm and the desired energy position of the peak is obtained. It should be noted that the low-energy peak in the latter calculation is associated with “cross” component of the source, while the higher-energy peak at about 13 MeV can be related to the “broom” correlation.

The systematics of the strength functions for peripheral sources for different q_α momentum transfers is illustrated in Fig. 7 (b). One may see that even the “peripheral assumption” is not sufficient to form a strong and distinct low-energy peak in the ${}^4\text{n}$ spectrum: the desired picture is realized only for certain intermediate range of transferred momenta $q_\alpha \sim 100 - 250$ MeV. This range well corresponds to situation of our experiment, see Fig. 5 and the related discussion in Section III.

The calculations for ${}^4\text{n}$ are performed up to $K_{\max} = 14$, which is insufficient for complete energy convergence. For that reason we perform simultaneously the calculations with advanced AV14 potential and simple central n - n potential BJ with much faster and “safer” convergence. The convergence curves are used for exponential extrapolation to infinite basis. For example, for calculations of Fig. 7 (a), the convergence point was 3.6 ± 0.12 MeV, while “underbinding” was ~ 1.4 MeV for AV14 and ~ 0.45 MeV for BJ potentials. For Fig. 9 the corresponding values are 2.7 ± 0.15 , ~ 1.8 and ~ 0.7 MeV. The additional control of the energy may be provided by phenomenological few-body potential with Fermi-function profile

$$V_A(\rho) = \frac{V_{A0}}{1 + \exp[(\rho - \rho_{A0})/d_{A0}]}. \quad (13)$$

The quite “soft” 4-body potential (13) with parameters $\rho_{40} = 12$ fm and $d_{40} = 3$ fm was used to get the peaks at $E_T(4n)$ energies pointed by the exponential extrapolation. “Safety” of the procedure in the sense of strength function shape was checked by $K_{\max} = 4 \rightarrow K_{\max} = 14$ extrapolations.

Qualitative comparison of theory and available data is provided in Fig. 8. Here we need to recall that strongly correlated picture of Fig. 7 is connected with $\sim 30\%$ of the ${}^8\text{He}$ WF projecting on the 0^+ state of ${}^4\text{n}$, while $\sim 70\%$ of this WF populate excited configurations of the ${}^4\text{n}$. The latter WF components are evaluated to provide strength function with maximum at 30 – 40 MeV, see thick gray curve in Fig. 8 (d). As we have mentioned in Section III, the information on transferred momenta is not available

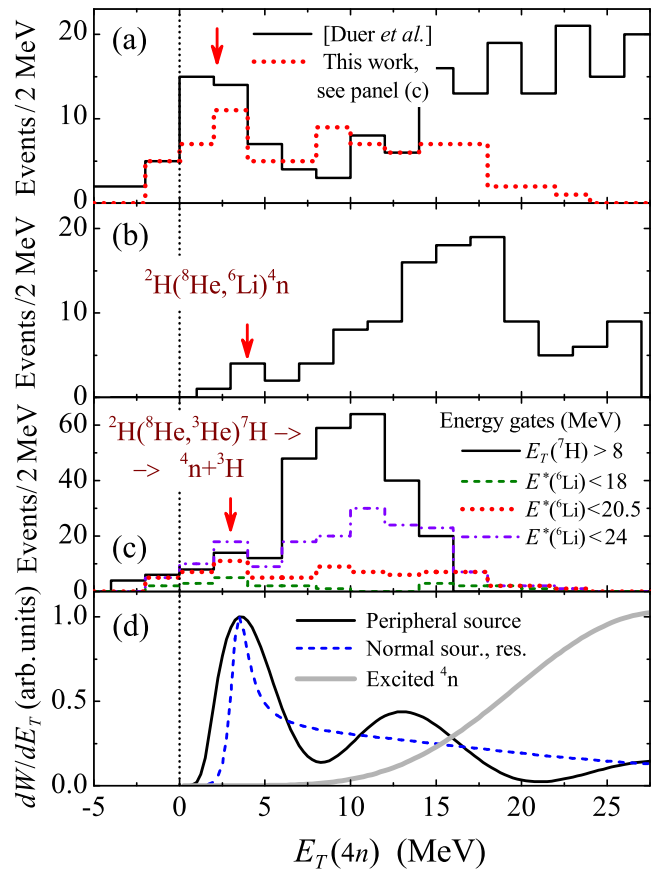


FIG. 8. Qualitative comparison of theory and data. (a) Data Duer *et al.* [6] plotted together with one of spectra panel (c). (b) Our data for the ${}^2\text{H}({}^8\text{He}, {}^6\text{Li}){}^4\text{n}$ reaction. (c) Our data for the ${}^2\text{H}({}^8\text{He}, {}^3\text{He}){}^7\text{H} \rightarrow {}^3\text{H} + {}^4\text{n}$ reaction for different selection conditions. (d) Theoretical results for $q_\alpha = 250$ MeV: nonresonant with peripheral source, resonant for normal source.

in Ref. [6], only the rough upper limit estimate $q_\alpha < 250$ MeV. This means that, so far, we can not find out even on the qualitative level, whether the experimental results of this work should be in principle, the same as in [6] (and they just seem somewhat different only because of experimental resolutions and statistics), or there should be some significant *physical* difference between them due to difference in the reaction mechanisms connected with q_α value.

It is also important to note that the low-energy peak connected with extreme peripheral source has very different profile compared to the case of the real resonant behavior connected with normal-size source. The “resonant” (blue dashed) curve in Fig. 8 (d) was generated by additional artificial binding introduced in Hamiltonian by phenomenological 4-body potential (13) with parameters $\rho_{40} = 7$ fm and $d_{40} = 1$ fm. The difference between “peripheral” black solid and “resonant” blue dashed curves in Fig. 8 (d) is too small to be seriously discussed for the available quality of the data. However, in principle,

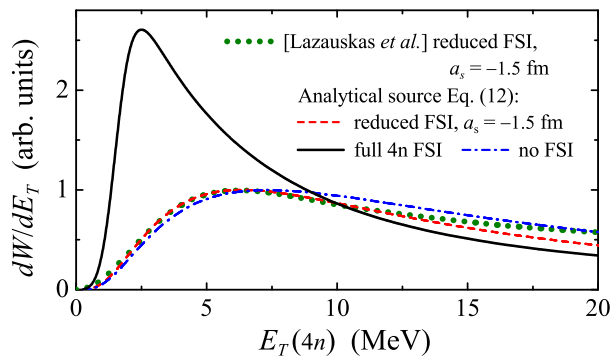


FIG. 9. Simulated computation by Lazauskas *et al.* [23]. Green dotted curve shows calculation with reduced n - n interaction from [23].

we have guidelines from theory how to distinguish experimentally the “peripheral” (caused by reaction mechanism) and “true resonant” tetra-neutron continuum responses.

VII. THEORETICAL DISCUSSION

In the recent paper [23] the data of [6] was qualitatively reproduced by emission off ${}^8\text{He}$ -induced source without any peripheral assumptions. This is in a strong contradiction to the results of [19] and this work. Let’s try to track the origin of this contradiction. In Fig. 3 of Ref. [23] a calculation with reduced n - n interaction (scattering length $a_s = -1.5$ fm) is shown. This calculation is reasonably close to “no FSI” situation and thus its origin could be to easier to “trace”. It is shown in Fig. 9 that a very close result is obtained in our calculations with simple analytical source

$$f_{\mathbf{q},K\gamma}(\rho_4) = \rho_4^\alpha \exp[-\rho_4/\rho_{40}], \quad \alpha = 1, \quad \rho_{40} = 3.85 \text{ fm}, \quad (14)$$

for the $K = 2, S = 0$ component. The rms neutron radius $\langle r_n \rangle = 3.34$ fm of such a source is very consistent with the values found in Table 3 of Ref. [23]. The strength function peak shape is somewhat different from that in Fig. 3 of [23], which indicates more complicated correlated nature of the source function in Ref. [23], then we assume in Eq. (14). However, the peak value for the full-calculation ${}^4\text{n}$ strength function in Fig. 9 well coincide with 2.5 MeV of [23], which means that we are reasonably “on a right track”.

So, in principle, there exist a class of source functions which can produce extreme low-energy peak in the ${}^4\text{n}$ spectrum for quite compact ($\langle r_n \rangle \sim 3$ fm) source. The only problem is that the “supersoft” source Eq. (14) has short-distance asymptotic $\sim \rho_4$. If we get back to the definition Eq. (8), this implies that ${}^8\text{He}$ overlap with 4-body hypersphericals is singular as $\sim \rho_4^{-3}$ at zero, which is highly unlikely for any realistic ${}^8\text{He}$ structure. The

${}^4\text{n}$ sources deduced in our work has asymptotic $\sim \rho_4^6$ at zero for $K = 2$; they can be reasonably approximated by expression like (14), but only for $\alpha = 6$. This is in full agreement with analytically deduced source functions of Ref. [19]. Consequently, such sources are much “harder” in the momentum space, and additional *peripheral assumption* is needed to get sizable low-energy effect in ${}^4\text{n}$ spectrum.

The origin of the “supersoft” source in [23] is probably due to the fact that ${}^4\text{n}$ c.m. is assumed to coincide with ${}^8\text{He}$ c.m. in Ref. [23] leading to several important inconsistencies:

- (i) This is an implicit assumption of infinitely heavy α -core in ${}^8\text{He}$ and, of course, quite a poor approximation considering the actual mass ratio of α and ${}^4\text{n}$.
- (ii) This also means that within the cluster model the charge radius of ${}^8\text{He}$ coincides with the charge radius of the α -particle, which contradicts to the corresponding experimental data [45].
- (iii) The “infinitely heavy core” assumption also leads to total absence of such an important characteristic as q_α in the formalism of [23]. In contrast, the “geometric” effects of ${}^4\text{n}$ motion relative to α in ${}^8\text{He}$ WF are found to be very pronounced in our calculations, see Fig. 6.
- (iv) The rms size of the source $\langle \rho_4 \rangle = 4.8$ fm, see e.g. Fig. 7 (a), presume significantly smaller $\langle r_n \rangle = 2.4$ fm distances in ${}^4\text{n}$ source, than the $\langle r_n \rangle$ distances in the initial ${}^8\text{He}$ WF, see Table II.

So, we insist that *peripheral assumption* is necessary to describe the extreme low-energy peak in the spectrum of ${}^4\text{n}$. This point is also qualitatively supported by extreme small cross sections for the observed peculiarities in the low-energy ${}^4\text{n}$ spectra. Typical cross section values for analogous direct reactions are some *millibarns* and even *tens of millibarns*, while we and Ref. [6] observe some *microbarns*. Such a cross section suppression looks quite natural if only the extreme periphery of the original ${}^4\text{n}$ configuration is actually participating in the reactions of interest *without destroying rescattering effects*.

VIII. CONCLUSION

Evidence for a hump in the ${}^4\text{n}$ continuum at 3.5 ± 0.7 and 3.2 ± 0.8 MeV was observed in the two reactions: ${}^2\text{H}({}^8\text{He}, {}^6\text{Li}){}^4\text{n}$ and ${}^2\text{H}({}^8\text{He}, {}^3\text{He}){}^7\text{H} \rightarrow {}^3\text{H} + {}^4\text{n}$, respectively. The ${}^4\text{n}$ peak energies in our work and the “resonance-like structure” energy 2.4 ± 0.6 MeV in Ref. [6] are consistent within experimental resolutions. We demonstrate that the reaction mechanism in both reported here cases is actually best interpreted as transfer reaction to the ground and to the ~ 18 MeV excited states of ${}^6\text{Li}$. The reaction mechanism also can be found reasonably consistent with that in the ${}^1\text{H}({}^8\text{He}, p){}^4\text{He} + {}^4\text{n}$ reaction [6], so it could be the same type of phenomenon. The statistics of 6 events for the first our reaction is quite low, but 26 – 40 events for the second one is comparable

to statistics connected with the low-energy ^4n resonance-like structure observed in [6].

Paper [23] is explaining the low-energy tetra-neutron peak in Ref. [6] as solely an initial state (^8He structure) effect in the presence of ^4n FSI. This is in a strong contradiction to the results of [19] and the results of this work. As compared to [19] the calculations of this work (i) are performed with realistic NN and $3N$ interactions, and (ii) the obtained realistic ^8He source demonstrates the complicated correlated behavior that is very important for the ^4n population. So far, the strong spatial correlations (Pauli focusing) for the ^8He g.s. WF has been several times discussed in the qualitative models [33, 47, 48], but in our work they are for the first time explicitly demonstrated in the realistic calculations of ^8He g.s. structure.

The two aspects mentioned above are not sufficient to fully explain the presence of a low-lying peak in the tetra-neutron spectrum. To do this, it is also necessary to consider extremely peripheral reaction mechanism, in which the α -core of ^8He interacts with the target, but four neutrons remain “spectators” at distances, far exceeding the typical sizes of neutron orbitals in ^8He . Using the appropriate profile function of the type Eq. (12), simulating such a geometry, it is possible to explain the presence of a low-lying peak in the tetra-neutron spectrum. Since the appearance of the low-energy peak is not related to the tetra-neutron *per se*, but also to the ISS (the source used) and the reaction mechanism, it should be expected that such a structure could be detected at somewhat different energies in different reactions. A possible reason of disagreement with the calculations [23] may be the incorrect ^4n c.m. treatment in the ^8He WF used in [23].

The existence of low-energy tetra-neutron *resonance* would mean a radical revision of everything we know about neutron-rich nuclei and neutron matter. Our vision of the problem is that a solution can be found, which is much less radical being related to the ^8He structure and reaction mechanisms. We got an important indication in our data that the ^4n spectrum is strongly dependent on the particular state of the recoil ^6Li system, which means, first of all, *on the reaction mechanism*. If our understanding of the low-energy structures in tetra-neutron is true, then it is actually not disappointing at all not to find tetra-neutron *resonance*: we get here an important cautionary lesson concerning low-energy observables in exotic nuclei and (for those interested) we arrive at a new exciting field of studies of extreme-peripheral phenomena in nuclear systems.

It is clear that the further studies of ^8He induced reactions on the deuteron target are needed to bring to full reliability the evidences obtained in this work. However, the processes of the major interest are all in the cross sections range of microbarns. Therefore, such studies make sense only if the statistical limitations of the existing data are overcome by about an order of magnitude, which is a real challenge for available experimental techniques and facilities.

Acknowledgments — This work was supported in part by the Russian Science Foundation (grant No. 22-12-00054). The research was supported in part in the framework of scientific program of the Russian National Center for Physics and Mathematics, topic number 6 “Nuclear and radiation physics” (2023-2025 stage). The authors are grateful to Prof. Yu.Ts. Oganessian for the long-term support of this research.

-
- [1] A. Baz and V. Bragin, *Physics Letters B* **39**, 599 (1972).
 [2] A. I. Baz’, V. I. Goldansky, V. Z. Goldberg, and Y. B. Zeldovich, *Light and intermediate nuclei near the border of nuclear stability* (Nauka, Moscow, 1972).
 [3] F. M. Marqués and J. Carbonell, *The European Physical Journal A* **57**, 105 (2021).
 [4] T. Faestermann, A. Bergmaier, R. Gernhäuser, D. Koll, and M. Mahgoub, *Physics Letters B* **824**, 136799 (2022).
 [5] K. Kismori, S. Shimoura, H. Miya, S. Michimasa, S. Ota, M. Assie, H. Baba, T. Baba, D. Beaumel, M. Dozono, T. Fujii, N. Fukuda, S. Go, F. Hammache, E. Ideguchi, N. Inabe, M. Itoh, D. Kameda, S. Kawase, T. Kawabata, M. Kobayashi, Y. Kondo, T. Kubo, Y. Kubota, M. Kurata-Nishimura, C. S. Lee, Y. Maeda, H. Matsubara, K. Miki, T. Nishi, S. Noji, S. Sakaguchi, H. Sakai, Y. Sasamoto, M. Sasano, H. Sato, Y. Shimizu, A. Stolz, H. Suzuki, M. Takaki, H. Takeda, S. Takeuchi, A. Tamii, L. Tang, H. Tokieda, M. Tsumura, T. Uesaka, K. Yako, Y. Yanagisawa, R. Yokoyama, and K. Yoshida, *Phys. Rev. Lett.* **116**, 052501 (2016).
 [6] M. Duer, T. Aumann, R. Gernhäuser, V. Panin, S. Paschalis, D. M. Rossi, N. Achouri, D. Ahn, C. A. Douma, F. Dufter, Z. Elekes, J. Feng, B. Fernández-Domínguez, U. Forsberg, N. Fukuda, I. Gasparic, Z. Ge, J. M. Gheller, J. Gibelin, A. Gillibert, K. I. Hahn, Z. Halász, M. N. Harakeh, A. Hirayama, M. Holl, N. Inabe, T. Isobe, J. Kahlbow, N. Kalantar-Nayestanaki, D. Kim, S. Kim, T. Kobayashi, Y. Kondo, D. Körper, P. Koseoglou, Y. Kubota, I. Kuti, P. J. Li, C. Lehr, S. Lindberg, Y. Liu, F. M. Marqués, S. Masuoka, M. Matsu-moto, J. Mayer, K. Miki, B. Monteagudo, T. Nakamura, T. Nilsson, A. Obertelli, N. A. Orr, H. Otsu, S. Y. Park, M. Parlog, P. M. Potlog, S. Reichert, A. Revel, A. T. Saito, M. Sasano, H. Scheit, F. Schindler, S. Shimoura, H. Simon, L. Stuhl, H. Suzuki, D. Symochko, H. Takeda, J. Tanaka, Y. Togano, T. Tomai, H. T. Törnqvist, J. Tscheuschner, T. Uesaka, V. Wagner, H. Yamada, B. Yang, L. Yang, Z. H. Yang, M. Yasuda, K. Yoneda, L. Zanetti, J. Zenihiro, and M. V. Zhukov, *Nature* **606**, 678 (2022).
 [7] S. C. Pieper, *Phys. Rev. Lett.* **90**, 252501 (2003-06).
 [8] N. K. Timofeyuk, *Journal of Physics G: Nuclear and Particle Physics*
 [9] M. D. Higgins, C. H. Greene, A. Kievsky, and M. Viviani, *Phys. Rev. C* **103**, 024004 (2021).
 [10] S. A. Sofianos, S. A. Rakityansky, and G. P. Vermaak, *Journal of Physics G: Nuclear and Particle Physics* **23**, 1619 (1997).

- [11] R. Lazauskas and J. Carbonell, *Phys. Rev. C* **72**, 034003 (2005).
- [12] S. Gandolfi, H.-W. Hammer, P. Klos, J. E. Lynn, and A. Schwenk, *Phys. Rev. Lett.* **118**, 232501 (2017).
- [13] K. Fossez, J. Rotureau, N. Michel, and M. Płoszajczak, *Phys. Rev. Lett.* **119**, 032501 (2017).
- [14] A. Deltuva, *Physics Letters B* **782**, 238 (2018).
- [15] A. Deltuva and R. Lazauskas, *Phys. Rev. C* **100**, 044002 (2019).
- [16] M. D. Higgins, C. H. Greene, A. Kievsky, and M. Viviani, *Phys. Rev. Lett.* **125**, 052501 (2020).
- [17] A. M. Shirokov, G. Papadimitriou, A. I. Mazur, I. A. Mazur, R. Roth, and J. P. Vary, *Phys. Rev. Lett.* **117**, 182502 (2016).
- [18] J. G. Li, N. Michel, B. S. Hu, W. Zuo, and F. R. Xu, *Phys. Rev. C* **100**, 054313 (2019).
- [19] L. V. Grigorenko, N. K. Timofeyuk, and M. V. Zhukov, *Eur. Phys. J. A* **19**, 187 (2004).
- [20] P. Hansen and B. Jonson, *Europhys. Lett.* **4**, 409 (1987).
- [21] C. Bertulani and G. Baur, *Nucl. Phys.* **A480**, 615 (1988).
- [22] L. V. Grigorenko, N. B. Shulgina, and M. V. Zhukov, *Phys. Rev. C* **102**, 014611 (2020).
- [23] R. Lazauskas, E. Hiyama, and J. Carbonell, *Phys. Rev. Lett.* **130**, 102501 (2023-03).
- [24] A. A. Bezbakh, V. Chudoba, S. A. Krupko, S. G. Belogurov, D. Biare, A. S. Fomichev, E. M. Gazeeva, A. V. Gorshkov, L. V. Grigorenko, G. Kaminski, O. A. Kiselev, D. A. Kostyleva, M. Y. Kozlov, B. Mauey, I. Mukha, I. A. Muzalevskii, E. Y. Nikolskii, Y. L. Parfenova, W. Piatek, A. M. Quynh, V. N. Schetinin, A. Serikov, S. I. Sidorchuk, P. G. Sharov, R. S. Slepnev, S. V. Stepantsov, A. Swiercz, P. Szymkiewicz, G. M. Ter-Akopian, R. Wolski, B. Zalewski, and M. V. Zhukov, *Phys. Rev. Lett.* **124**, 022502 (2020).
- [25] I. A. Muzalevskii, A. A. Bezbakh, E. Y. Nikolskii, V. Chudoba, S. A. Krupko, S. G. Belogurov, D. Biare, A. S. Fomichev, E. M. Gazeeva, A. V. Gorshkov, L. V. Grigorenko, G. Kaminski, O. Kiselev, D. A. Kostyleva, M. Y. Kozlov, B. Mauey, I. Mukha, Y. L. Parfenova, W. Piatek, A. M. Quynh, V. N. Schetinin, A. Serikov, S. I. Sidorchuk, P. G. Sharov, N. B. Shulgina, R. S. Slepnev, S. V. Stepantsov, A. Swiercz, P. Szymkiewicz, G. M. Ter-Akopian, R. Wolski, B. Zalewski, and M. V. Zhukov, *Phys. Rev. C* **103**, 044313 (2021).
- [26] E. Y. Nikolskii, I. A. Muzalevskii, A. A. Bezbakh, V. Chudoba, S. A. Krupko, S. G. Belogurov, D. Biare, A. S. Fomichev, E. M. Gazeeva, A. V. Gorshkov, L. V. Grigorenko, G. Kaminski, M. Khirk, O. Kiselev, D. A. Kostyleva, M. Y. Kozlov, B. Mauey, I. Mukha, Y. L. Parfenova, W. Piatek, A. M. Quynh, V. N. Schetinin, A. Serikov, S. I. Sidorchuk, P. G. Sharov, N. B. Shulgina, R. S. Slepnev, S. V. Stepantsov, A. Swiercz, P. Szymkiewicz, G. M. Ter-Akopian, R. Wolski, B. Zalewski, and M. V. Zhukov, *Phys. Rev. C* **105**, 064605 (2022).
- [27] E. Nikolskii, I. Muzalevskii, S. Krupko, A. Bezbakh, V. Chudoba, S. Belogurov, D. Biare, A. Fomichev, E. Gazeeva, A. Gorshkov, L. Grigorenko, G. Kaminski, M. Khirk, O. Kiselev, D. Kostyleva, M. Kozlov, B. Mauey, I. Mukha, Y. Parfenova, A. Quynh, V. Schetinin, A. Serikov, S. Sidorchuk, P. Sharov, R. Slepnev, S. Stepantsov, A. Swiercz, G. Ter-Akopian, R. Wolski, and M. Zhukov, *Nuclear Instruments and Methods in Physics Research Section B: Beam Interactions with Materials and Atoms* **541**, 121 (2023).
- [28] E. Y. Nikolskii, S. A. Krupko, I. A. Muzalevskii, A. A. Bezbakh, R. Wolski, C. Yuan, S. G. Belogurov, D. Biare, V. Chudoba, A. S. Fomichev, E. M. Gazeeva, M. S. Golovkov, A. V. Gorshkov, L. V. Grigorenko, G. Kaminski, M. Khirk, O. Kiselev, D. A. Kostyleva, B. Mauey, I. Mukha, Y. L. Parfenova, A. M. Quynh, S. I. Sidorchuk, P. G. Sharov, N. B. Shulgina, R. S. Slepnev, S. V. Stepantsov, A. Swiercz, and G. M. Ter-Akopian, *Physics of Atomic Nuclei* **86**, 923 (2023).
- [29] I. A. Muzalevskii, A. A. Bezbakh, E. Y. Nikolskii, V. Chudoba, A. M. Abakumov, S. A. Krupko, S. G. Belogurov, D. Biare, A. S. Fomichev, E. M. Gazeeva, A. V. Gorshkov, L. V. Grigorenko, G. Kaminski, O. Kiselev, D. A. Kostyleva, B. Mauey, I. Mukha, A. M. Quynh, S. I. Sidorchuk, N. B. Shulgina, R. S. Slepnev, A. Swiercz, G. M. Ter-Akopian, R. Wolski, and M. V. Zhukov, *EPJ Web of Conferences* **290**, 09001 (2023).
- [30] A. A. Bezbakh, S. G. Belogurov, R. Wolski, E. M. Gazeeva, M. S. Golovkov, A. V. Gorshkov, G. Kaminski, M. Y. Kozlov, S. A. Krupko, I. A. Muzalevskii, E. Y. Nikolskii, E. V. Ovcharenko, R. S. Slepnev, G. M. Ter-Akopian, A. S. Fomichev, P. G. S. V. Chudoba, and V. N. Schetinin, *Instruments and Experimental Techniques* **61**, 631 (2018).
- [31] E. Rich, S. Fortier, D. Beamel, E. Becheva, Y. Blumenfeld, F. Delaunay, N. Ffrascaria, S. Gales, J. Guillot, F. Hammache, E. Khan, V. Lima, B. Pothet, J.-A. Scarpaci, O. Sorlin, E. Tryggerstadt, R. Wolski, A. Gillibert, V. Lapoux, L. Nalpas, A. Obertelli, E. Pollaco, F. Skaza, P. Roussel-Chomaz, A. Fomichev, S. Stepantsov, and D. Santonocito, in *Proc. of Int. Conf. Exotic Nuclei Exon2004*, edited by Y. Penionzhkevich (World Scientific, Peterhof, Russia, 2005) pp. 36–44.
- [32] S. Fortier, E. Tryggestad, E. Rich, D. Beamel, E. Becheva, Y. Blumenfeld, F. Delaunay, A. Drouart, A. Fomichev, N. Frascaria, S. Gales, L. Gaudefroy, A. Gillibert, J. Guillot, F. Hammache, K. W. Kemper, E. Khan, V. Lapoux, V. Lima, L. Nalpas, A. Obertelli, E. C. Pollacco, F. Skaza, U. D. Pramanik, P. Roussel-Chomaz, D. Santonocito, J. A. Scarpaci, O. Sorlin, S. V. Stepantsov, G. M. Ter Akopian, and R. Wolski, *AIP Conference Proceedings* **912**, 3 (2007), <https://aip.scitation.org/doi/pdf/10.1063/1.2746575>.
- [33] P. Sharov, L. Grigorenko, A. Ismailova, and M. Zhukov, *JETPh Lett.* **110**, 5 (2019).
- [34] D. Tilley, C. Cheves, J. Godwin, G. Hale, H. Hofmann, J. Kelley, C. Sheu, and H. Weller, *Nucl. Phys.* **A708**, 3 (2002).
- [35] M. V. Zhukov, B. Danilin, D. Fedorov, J. Bang, I. Thompson, and J.S.Vaagen, *Phys. Rep.* **231**, 151 (1993).
- [36] L. V. Grigorenko, T. D. Wiser, K. Mercurio, R. J. Charity, R. Shane, L. G. Sobotka, J. M. Elson, A. H. Wuosmaa, A. Banu, M. McCleskey, L. Trache, R. E. Tribble, and M. V. Zhukov, *Phys. Rev. C* **80**, 034602 (2009).
- [37] S. Sack, L. C. Biedenharn, and G. Breit, *Phys. Rev.* **93**, 321 (1954).
- [38] S. Neumaier, G. Alkhazov, M. Andronenko, A. Dobrovolsky, P. Egelhof, G. Gavrilov, H. Geissel, H. Irnich, A. Khanzadeev, G. Korolev, A. Lobodenko, G. Munzenberg, M. Mutterer, W. Schwaba, D. Seliverstov, T. Suzuki, N. Timofeev, A. Vorobyov, and V. Yatsoura, *Nuclear Instruments and Methods in Physics Research Section B: Beam Interactions with Materials and Atoms* **541**, 121 (2023).

- [39] I. Tanihata, H. Hamagaki, O. Hashimoto, S. Nagamiya, Y. Shida, N. Yoshikawa, O. Yamakawa, K. Sugimoto, T. Kobayashi, D. Greiner, N. Takahashi, and Y. Nojiri, *Phys. Lett. B* **160**, 380 (1985).
- [40] R. B. Wiringa, V. G. J. Stoks, and R. Schiavilla, *Phys. Rev. C* **51**, 38 (1995).
- [41] G. E. Brown and A. D. Jackson, *The nucleon–nucleon interaction* (North-Holland, Amsterdam, 1976).
- [42] E. Hiyama, B. F. Gibson, and M. Kamimura, *Phys. Rev. C* **70**, 031001 (2004).
- [43] R. B. Wiringa, S. C. Pieper, J. Carlson, and V. R. Pandharipande, *Phys. Rev. C* **62**, 014001 (2000).
- [44] S. C. Pieper, R. B. Wiringa, and J. Carlson, *Phys. Rev. C* **70**, 054325 (2004).
- [45] P. Mueller, I. A. Sulai, A. C. C. Villari, J. A. Alcántara-Núñez, R. Alves-Condé, K. Bailey, G. W. F. Drake, M. Dubois, C. Eléon, G. Gaubert, R. J. Holt, R. V. F. Janssens, N. Lescsne, Z.-T. Lu, T. P. O’Connor, M.-G. Saint-Laurent, J.-C. Thomas, and L.-B. Wang, *Phys. Rev. Lett.* **99**, 252501 (2007).
- [46] J. J. Krauth, K. Schuhmann, M. A. Ahmed, F. D. Amaro, P. Amaro, F. Biraben, T.-L. Chen, D. S. Covita, A. J. Dax, M. Diepold, L. M. P. Fernandes, B. Franke, S. Galtier, A. L. Gouvea, J. Gotzfried, T. Graf, T. W. Hansch, J. Hartmann, M. Hildebrandt, P. Indelicato, L. Julien, K. Kirch, A. Knecht, Y.-W. Liu, J. Machado, C. M. B. Monteiro, F. Mulhauser, B. Naar, T. Nebel, F. Nez, J. M. F. dos Santos, J. P. Santos, C. I. Szabo, D. Taqqu, J. F. C. A. Veloso, J. Vogelsang, A. Voss, B. Weichelt, R. Pohl, A. Antognini, and F. Kottmann, *Nature* **589**, 527 (2021).
- [47] M. V. Zhukov, A. A. Korshennikov, and M. H. Smedberg, *Phys. Rev. C* **50**, R1 (1994).
- [48] P. Mei and P. V. Isacker, *Annals of Physics* **327**, 1162 (2012).